

## RESEARCH ARTICLE

# Design of a Compact Dual-Band Right-Hand Circularly Polarized Antenna on Magnetized Ferrite Substrate for L-Band Applications

WRIDDHI BHOWMIK<sup>1</sup>, JEHISON LEON VALDES<sup>2</sup>, THIERRY MONEDIERE<sup>2</sup>,  
AND LAURE HUITEMA<sup>2,3</sup>, (Member, IEEE)

<sup>1</sup>Kalinga Institute of Industrial Technology, Bhubaneswar, Odisha 751024, India

<sup>2</sup>XLIM Research Institute, CNRS, University of Limoges, 87060 Limoges, France

<sup>3</sup>Institut Universitaire de France (IUF), 75005 Paris, France

Corresponding author: Wriddhi Bhowmik (wriddhi.bhowmikfet@kiit.ac.in)

This work was supported by the [PLATeforme de technologie et d'INstrumentation pour l'Optique et les Microondes (PLATINOM) Technology and Instrumentation Platform for Optics and Microwaves] Platform (www.unilim.fr\platinom) funded by the European Regional Development Foundation and the French Government with the New Aquitaine Region under Grant FEDER-PILIM 2015-2020.

**ABSTRACT** This article presents the design of a dual-band right-hand circularly polarized microstrip patch antenna on a magnetized ferrite substrate for the L-band (1 GHz - 2 GHz) applications. The magnetization of the ferrite material enables the antenna to resonate with counter-rotating modes at successive multiband frequencies. In this paper, a unique structure consisting of two stacked ferrite substrates with two different internal dc magnetic fields is used to obtain identical circular polarization modes at two relatively close operating frequencies. In addition, the use of a ferrite material allows the overall dimensions of the antenna to be reduced to approximately  $\lambda_0/9.4 \times \lambda_0/9.4 \times \lambda_0/23$  at 1.227 GHz thanks to the high permittivity and high effective permeability of this kind of materials. The antenna exhibits only right-hand circular polarization (RHCP) with good axial ratio (AR) at 1.227 GHz and 1.575 GHz within the L-band. The antenna performs well in both simulations and measurements.

**INDEX TERMS** Dual-band, polder permeability tensor, right-hand circular polarization, saturated ferrite material.

## I. INTRODUCTION

Circularly polarized (CP) antennas are highly effective in mitigating the multipath effect. They also eliminate the dependence on the orientation of the transmitting and receiving antennas, thereby reducing transmission losses caused by polarization mismatch. Multiband CP antennas have garnered significant attention for use in mobile terminals. Typically, Right-Hand Circular Polarization (RHCP) is favored to minimize multipath losses. However, designing a compact dual-band RHCP antenna poses considerable challenges.

The development of circularly polarized (CP) microstrip patch antennas has been extensively explored. In the literature, they can be classified into single-feed single-band [1], [2], [3], [4], [5], single-feed dual-band [1], [6], [7], [8],

[9], [10], dual-feed dual-band [11], single-band with feeding networks [12], and dual-band with feeding networks [13], [14], [15]. Representative designs from each category are summarized in the introduction for better clarity. In [3], a square patch antenna with dimensions  $\lambda_0/3.26 \times \lambda_0/3.26 \times \lambda_0/125$  at 1.575 GHz achieved CP through four sequential asymmetrical slits, with corner truncation improving the axial ratio bandwidth and a center cross slot enabling miniaturization. A cross-shaped rectangular patch antenna with dimensions  $\lambda_0/5.4 \times \lambda_0/3.9 \times \lambda_0/59.5$  at 1.575 GHz is presented in [5], which achieves CP by embedding a 'V'-shaped slot at its center. In [6], a stacked design features an asymmetric annular slot antenna on the lower substrate's bottom layer and a metasurface on the upper substrate's top layer. The slot achieves CP at 2.5 GHz, while the stacked metasurface generates CP at 3.5 GHz. A single-fed dual-band CP antenna with dimensions  $\lambda_0/1.76 \times \lambda_0/$

The associate editor coordinating the review of this manuscript and approving it for publication was Tutku Karacolak<sup>1</sup>.

$1.76 \times \lambda_0/43.7$  at 1.227 GHz, presented in [9], achieved CP by incorporating a cross slot at the center of the square patch antenna. In [10], a square patch antenna with a center slot achieves CP over two frequency bands by integrating either four “T”-shaped slits at its edges or four “Y”-shaped slits at its corners, facilitating design miniaturization. In [11], a dual-band CP antenna uses a quadrature hybrid coupler to excite two feeds of a slotted patch with equal magnitude and a  $90^\circ$  phase difference. In [12], a single-band CP antenna achieves circular polarization through a feeding network that includes a quadrature coupler, dual lumped capacitors, and an impedance matching line. A compact quadruple inverted-F antenna is presented in [14], achieving CP through quadrature excitation of the antenna elements via a lossless phase quadrature feeding network. In [15], a stacked dual-band CP patch antenna uses a microstrip feeding network and aperture coupling to generate CP. Multiple feeds are also used in [16] to increase polarization purity and pattern symmetry.

Single-feed dual-band CP antennas often require extensive parametric analysis of the design parameters in order to excite two orthogonal modes with equal amplitude and quadrature phase for CP generation. These parametric studies [6], [9], [10] make the design process both complex and time-consuming. Multiple excitation of the radiating elements (via a feeding network) provides good circular polarization, but often requires a large ground plane, resulting in additional losses and higher manufacturing costs.

Polarized ferrite materials offer a compelling alternative because, when biased with a DC magnetic field, they naturally exhibit anisotropy and non-reciprocity, enabling the generation of CP waves without the need for complex feeding networks [17], [18], [19], [20]. Their relatively high permeability ( $\mu > 1$ ) and high permittivity ( $\epsilon \approx 12$ – $16$ ) also make them particularly suitable for antenna miniaturization [21], [22]. Prior works [21], [22], [23] have demonstrated that ferrite-based patch antennas can achieve compactness and good-quality CP performance. However, two main drawbacks persist: (i) the operating frequencies cannot be independently selected, and (ii) in multi-band configurations, the circular polarization alternates (right or left) depending on the excited mode ( $TM_{-11}$  or  $TM_{+11}$ ) [24]. For example, [22] reported a ferrite antenna operating on three frequency bands, but with alternating RHCP and LHCP radiation. These limitations highlight the difficulty of achieving identical polarization across closely spaced frequency bands using a single ferrite resonator.

The proposed antenna specifically targets the L-band (1.227 GHz and 1.575 GHz), which is widely used in satellite-based navigation and communication systems such as GPS, Galileo, and BeiDou. These systems strictly require RHCP radiation at all operating frequencies to ensure robust signal reception and minimize losses due to multipath and polarization mismatch. To meet this application requirement, this paper presents a novel dual-band RHCP antenna for the L-band. The proposed design integrates antenna miniaturization, dual-band RHCP operation, and fabrication feasibility.

By employing two stacked ferrite substrates, it achieves identical RHCP modes at two closely spaced frequencies, providing a practical and efficient solution for L-band satellite applications. The main contributions of this work can be summarized as follows:

- i Excitation of only RHCP modes at consecutive resonance frequencies in the strong field area of a magnetized ferrite substrate.
- ii Control of the static magnetic field in a double-level structure.
- iii The possibility of obtaining a dual-band RH circularly polarized antenna with closely spaced frequency bands ( $f_2/f_1 = 1.27$ ).
- iv Utilization of ferrite material in the strong field region, where its permeability exceeds one, enabling antenna size reduction and miniaturization.

In section II, the theoretical analysis of a circular patch antenna using a saturated ferrite material is discussed. This initial study helps determine the resonator configuration and dimensions. Section III covers the simulation of the antenna with a homogeneous magnetic field inside the ferrite, followed by a magnetostatic study with permanent magnets and electromagnetic/magnetostatic co-simulation to precisely determine the antenna design. All simulations are performed using CST Microwave Studio software [25]. Sections IV and V respectively present the fabricated prototype and corresponding measurement results, validating the generation of right-hand circularly polarized (RHCP) modes in the L-band. Additionally, section V compares the proposed antenna’s dimensions and performance with previously reported ferrite and non-ferrite antennas in the literature. Section VI concludes the study.

## II. THEORETICAL ANALYSIS

The anisotropic and non-reciprocal behavior of the ferrite material enables circular polarization to be obtained when it is subjected to a DC magnetic field. The permeability of the ferrite material can be represented by the Polder tensor, when the magnetic field applied to the ferrite along the z axis is sufficient to saturate the material. This tensor is expressed as Eq. (1) [22].

$$[\mu_r(\omega)] = \begin{bmatrix} \mu & -j\kappa & 0 \\ j\kappa & \mu & 0 \\ 0 & 0 & 1 \end{bmatrix} \quad (1)$$

where the elements of the permeability tensor are determined by Eq. (2) and Eq. (3).

$$\mu = 1 + \frac{\omega_m \omega_0}{\omega_0^2 - \omega^2} = \mu' - j\mu'' \quad (2)$$

$$\kappa = \frac{\omega_m \omega}{\omega_0^2 - \omega^2} = \kappa' - j\kappa'' \quad (3)$$

Here,  $\omega = 2\pi f$ , while  $\omega_m$  is the gyrotropic frequency and  $\omega_0$  is the Larmor frequency, given by Eq. (4) and Eq. (5), respectively.

$$\omega_m = \gamma \mu_0 M_s \quad (4)$$

$$\omega_0 = \gamma \mu_0 H_i + j\omega\alpha \quad (5)$$

Hence, it can be observed from the above equations that the elements of the permeability tensor depend on the internal DC magnetic bias field  $H_i$ , the saturation magnetization of ferrite  $M_s$ , and the frequency  $f$ . The gyromagnetic ratio  $\gamma$  is defined as  $\gamma = 2.8 \text{ MHz/Oe}$ . The magnetic losses of the ferrite material are taken into account by the coefficient  $\alpha$ , defined by Eq. (6).

$$\alpha = \frac{\gamma \Delta H}{2f} \tag{6}$$

where  $\Delta H$  is the ferrite line width. The gyromagnetic resonance is given by Eq. (7).

$$f_r = \gamma H_i \tag{7}$$

Fig. 1 plots the Polder tensor's elements as a function of frequency. This plot clearly distinguishes the strong-field region, the weak-field region, and the gyromagnetic resonance (GMR). The strong-field region occurs before the gyromagnetic resonance, while the weak-field region appears beyond it.  $\text{Re}(\mu) > 1$  in the strong field area enables antenna miniaturization. The magnetic losses are very high around gyromagnetic resonance (GMR).

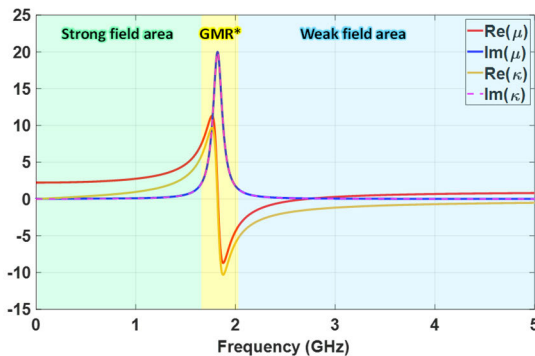


FIGURE 1. Evolution of Polder tensor's elements as the function of frequency for Y39 ferrite material with  $H_i = 650 \text{ Oe}$ . \*GMR: gyromagnetic resonance.

In the interest of miniaturization, the operation of the proposed resonators will be within the strong field zone (below the gyromagnetic resonance). The modal study of a ferrite patch antenna has been recently detailed in [22] and [23] and based on this study, the evolution of the resonance frequencies of the  $TM_{\pm 11}$  modes as a function of internal DC magnetic field for a circular patch antenna with a radius of  $a = 11.6 \text{ mm}$  on a Y39 ferrite substrate is plotted in Fig. 2.

The cavity model analysis shows that, for a given bias field, only one RHCP and one LHCP mode can resonate in the strong field area. The primary research objective is to eliminate the LHCP mode and obtain two RHCP modes at closely spaced frequencies in the strong field area, using a miniaturized antenna for L-band applications. The antenna proposed for this purpose comprises two circular patches on two separate ferrite substrates, biased with two different magnetic fields to obtain the two RHCP modes. No previous

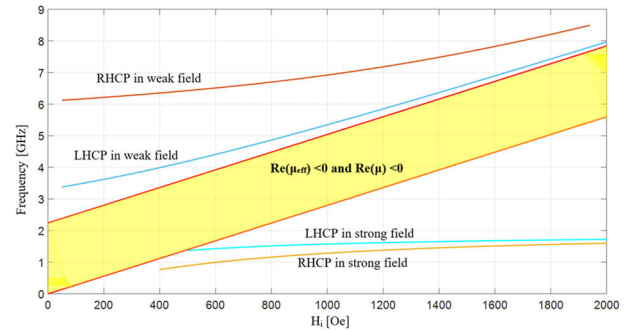


FIGURE 2. Evolution of resonance frequencies of  $TM_{\pm 11}$  modes versus the internal DC magnetic field with  $a = 11.6 \text{ mm}$ ,  $4\pi M_s = 800 \text{ Gauss}$ , and  $\epsilon_r = 14.6$ .

work has been reported using two stacked ferrite substrates. The proximity coupling method was chosen to excite the antenna in order to avoid drilling through the ferrite substrate as well as the bottom magnet.

Therefore, in the following, only the RHCP modes operating in the strong-field region will be considered. The LHCP modes, which are expected to occur just above these frequencies, will not be further analyzed as long as they remain outside the frequency bands of interest. The next section presents the antenna design and the simulation process, including the magnetostatic study and the magneto-static/electromagnetic co-simulation.

### III. DESIGN AND SIMULATION OF THE ANTENNA

In order to obtain RHCP modes at close frequencies, the design consists of two stacked circular ferrite resonators. One of the resonators has its first RHCP mode at  $1.227 \text{ GHz}$ , and the second resonator at  $1.575 \text{ GHz}$ . The bottom resonator consists of a ferrite disk inserted in an alumina ring. This geometry facilitates the magnetization of the ferrite to saturation using permanent magnets placed on either side of the antenna (Fig. 3(b)). The modes are excited by proximity coupling, requiring the smaller of the two resonators to be placed at the top of the structure. The DC magnetic field is provided by magnets placed on the top and bottom of the device.

Fig. 3(a) shows that a fully ferrite resonator 1 cannot be (due to the edge effect) magnetically saturated. Partial magnetization requires empirical, non-predictive tensors (Rado [26], Green & Sandy [27], Igarashi & Naito [28], [29]). To bypass this, a dielectric ring is added around the lower resonator, enabling full ferrite saturation by magnets 1 and 2 (Fig. 3(b)). The dielectric chosen is alumina to have a permittivity close to that of the ferrite.

The metallic patch element is then integrated on top of each ferrite. These two patch antennas are excited by proximity coupling on their first  $TM_{-11}$  mode in order to generate a right-hand circular polarization. The proximity coupling of the resonator 1 is achieved by a simple microstrip line etched on a plate of a Rogers RT 5880 substrate, which also

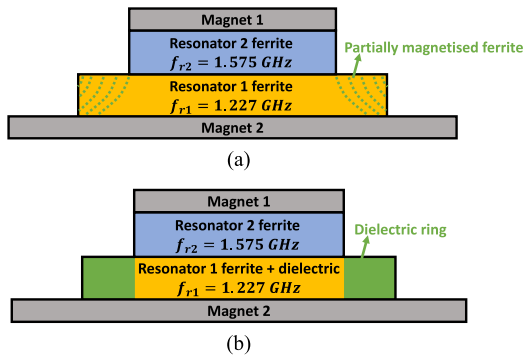


**FIGURE 3.** (a) Typical stacking of magnets and resonators composed exclusively of ferrite, and (b) approach implemented to avoid partially magnetized ferrites: addition of a dielectric ring around the bottom ferrite.

incorporates the antenna ground plane. The ground plane size (50 mm × 50 mm) was carefully chosen as a compromise between reducing measurement perturbations and maintaining the compact dimensions of the antenna. Indeed, this ground plane helps reduce the influence of the measurement setup and surrounding environment, while still allowing compact antenna integration. Excitation of the upper resonator (resonator 2) is achieved by etching a slot in the lower patch antenna.

**A. SIMULATION USING A HOMOGENEOUS INTERNAL DC MAGNETIC FIELD**

The antenna design is depicted in Fig. 4.

Resonator 1 consists of a cylindrical ferrite disc with a height of 3.5 mm and a radius of 11.3 mm, inserted in a cylindrical alumina ring, also with a height of 3.5 mm and outer and inner radii of 15 mm and 11.3 mm, respectively (Fig. 4 (a) and (c)). The metallic top-hat of the resonator 1 has a radius of 13 mm, in which a slot is etched to allow excitation of the  $TM_{-11}$  mode of the second resonator. Due to its geometry and dimensions, this slot allows magnetic coupling and matching around 1.575 GHz for the resonator 2 (with a height and radius of 5.5 mm and 11.6 mm, respectively, as shown in Fig. 4 (a) and (b)).

The stacked patches have been placed at the center of a rectangular (50 mm × 50 mm) dielectric substrate (Rogers RT5880) (Fig. 4 (a)). The proximity coupling-based excitation of the lower resonator is achieved by designing a 50 Ω feeding line with a width and length of 2.5 mm and 20 mm, respectively (Fig. 4 (d)).

The Y39 ferrite material is a suitable option to be used in the strong field area, as the material has a low effective resonance linewidth,  $\Delta H_{eff} = 4$  Oe, a saturation magnetization  $4\pi M_s = 800$  Gauss, and a dielectric permittivity  $\epsilon_r = 14.6$  with  $\tan\delta = 2 \times 10^{-4}$ .

The dielectric constants and loss tangents of alumina and Rogers RT5880 are 9.4 and 2.2, and  $4 \times 10^{-4}$  and  $9 \times 10^{-4}$ , respectively. Based on the cavity model analysis (Fig. 2), the internal magnetic field  $H_i$  is fixed to 620 Oe inside the lower ferrite and 650 Oe inside the upper ferrite to excite the

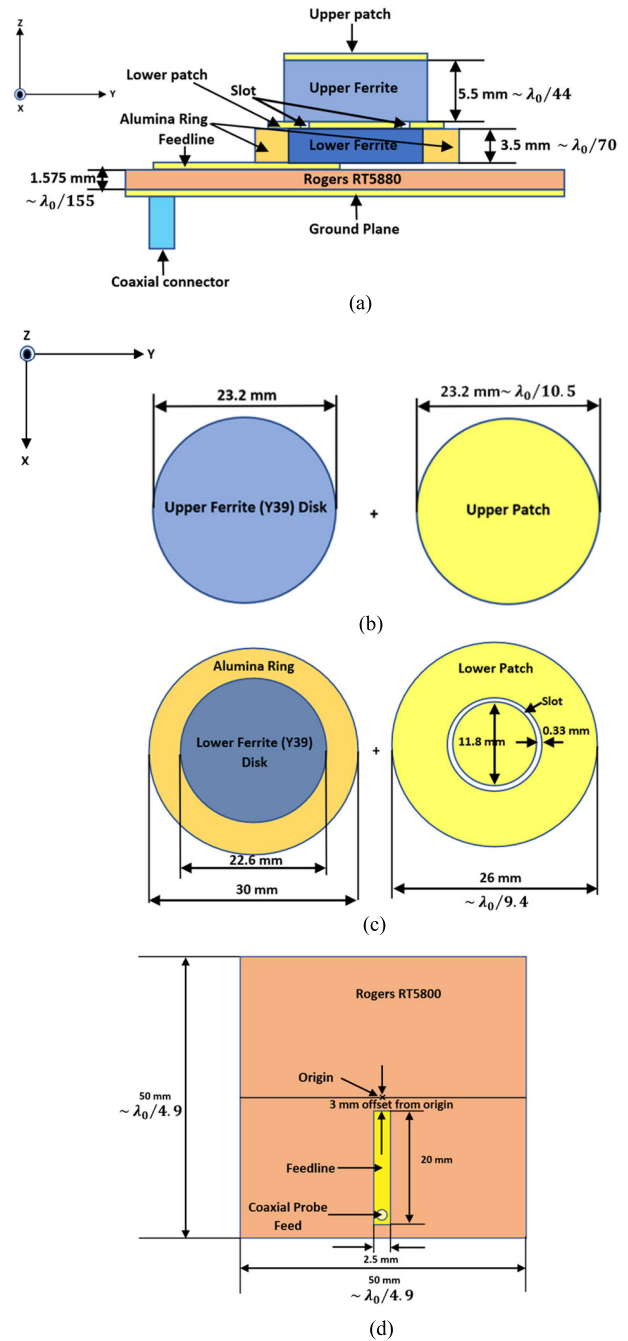


**FIGURE 4.** Layout: (a) side view of the proposed antenna, top view: (b) upper patch, (c) lower patch, and (d) proximity coupling.

RHCP modes at 1.227 GHz and 1.575 GHz respectively. This preliminary study represents an ideal case where the  $H_i$  field is considered homogeneous within the ferrites. It provides an initial dimensioning of the structure. This study will then need to be completed by a magnetostatic study, which will integrate the real DC magnetic field applied by magnets on either side of the ferrites.

The diameter of the upper ferrite must be greater than or equal to the diameter of the lower ferrite for the real-time magnetization (using permanent magnets) of the

ferrite materials. Therefore, to satisfy this criterion, the radius of the upper ferrite was set to 11.6 mm, while the radius of the lower ferrite was set to 11.3 mm. To achieve resonance around 1.227 GHz, the radius of the lower metal top-hat (13 mm) is larger than the radius of the lower ferrite (11.3 mm). Therefore, to accommodate the patch, the need for extra space was met by embedding the ferrite disc inside the alumina ring, which can be considered a unique approach, as this type of antenna design has not been reported before.

Fig. 5 shows the  $|S_{11}|$  parameter and the boresight axial ratio (AR) as a function of frequency on the same graph to verify whether the matching bands correspond to the frequency bands where the AR is minimal. As one of the aims of this work is to miniaturize antennas, a matching criterion of  $-6$  dB is used.

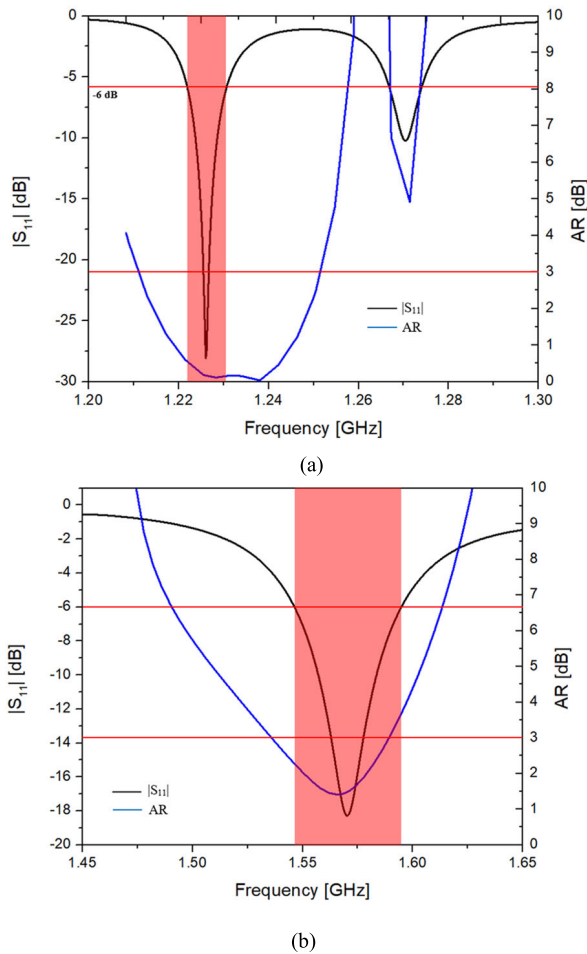


**FIGURE 5.**  $|S_{11}|$  and AR of the proposed antenna for an homogeneous magnetic field inside the ferrite material: (a) 620 Oe inside lower ferrite, and (b) 650 Oe inside the upper ferrite.

Satisfactory impedance matching is achieved at both frequencies, with an axial ratio (AR) well below 3 dB at the frequency where the  $|S_{11}|$  parameter is minimal (the AR values are 0.16 dB at 1.227 GHz and 1.47 dB at 1.575 GHz). As discussed earlier, the operation in the strong field makes the antenna compact since the dimensions of the proposed

antenna are  $\lambda_0/9.4 \times \lambda_0/9.4 \times \lambda_0/23$  at 1.227 GHz. Fig. 6 presents the normalized circularly polarized radiation patterns of the antenna and shows that the antenna operates on the  $TM_{-11}$  mode for both frequencies. Indeed, the RHCP gain is much higher than the LHCP gain and exhibits boresight radiation.

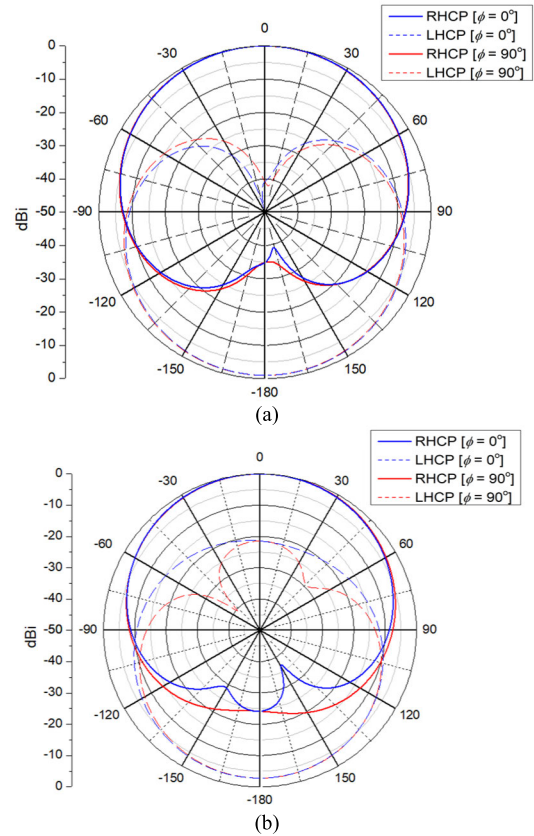


**FIGURE 6.** Normalized radiation patterns for  $\phi = 0^\circ$  (xOz-plane) and  $\phi = 90^\circ$  (yOz-plane): (a) at 1.227 GHz, and (b) at 1.575 GHz.

The boresight realized gains and radiation efficiencies of the antenna are  $-0.857$  dBi and 41% respectively for the first RHCP mode (1.227 GHz), and 2.86 dBi and 75%, respectively for the second RHCP mode (1.575 GHz). As the antenna is more miniaturized on the first mode than on the second RHCP mode, it is expected for the radiation efficiency and gain to be lower at this operating frequency.

This ideal case study shows that the simulation of the proposed antenna with an appropriately homogeneous magnetic field bias inside the ferrite material generates RHCP modes at the desired frequency bands. The antenna also radiates behind the ground plane due to its small size in comparison to the wavelength, and of course, the polarization is inverted behind the antenna. The next step is to simulate the proposed antenna using a real magnetic field, i.e., a magnetic field generated by a magnet. This will enable us to determine and select the properties of the magnets to be integrated.

The magnets will have to create an internal magnetic field close to 620 Oe and 650 Oe inside the lower and upper ferrite

substrates, respectively, to obtain antenna performance that approximates the ideal case. This step will be carried out by means of a magnetostatic/electromagnetic co-simulation of the antenna and represents a crucial stage in the manufacture and measurement of the prototype.

### B. MAGNETOSTATIC SIMULATION

To generate an accurate internal magnetic field  $H_i$  inside the ferrite materials using permanent magnets, a magnetostatic simulation of the proposed design was carried out. Two commercial permanent magnets of cylindrical shape [30] were used to magnetize the ferrite materials. One magnet was placed above the upper patch, and another magnet was positioned below the ground plane. A parametric study was conducted on the dimensions of the magnets and their residual flux densities in order to obtain a precise magnetic field inside the ferrite material, following the process previously described in [31]. Samarium-Cobalt magnets were used with the top magnet having a residual flux density  $B_{r1} = 1.1 T$ , a radius of 11.6 mm and a height of 1.9 mm, and the bottom magnet having a residual flux density  $B_{r2} = 1.08 T$ , a radius of 14 mm and a height of 3.2 mm. To reduce the inhomogeneity of the magnetic field inside the ferrite material, two steel plates were introduced. The first steel plate (with a radius and height of 11.6 mm and 0.5 mm, respectively) was placed between the upper patch and the upper magnet, while the second steel plate (with a radius and height of 14 mm and 0.5 mm, respectively) was positioned between the ground plane and the lower magnet. The complete design is presented in Fig. 7.

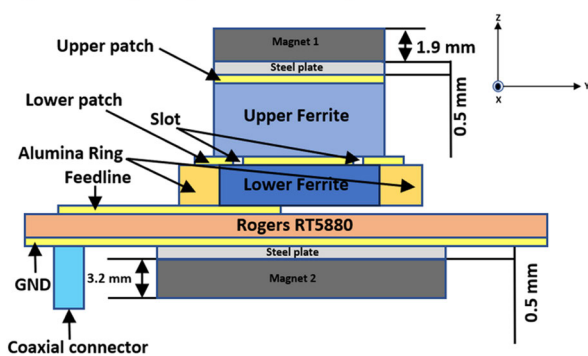


FIGURE 7. Side view of the antenna with magnets and steel plates.

The magnetostatic analysis of the antenna using these permanent magnets was successfully completed, and 3D representations of the magnetic field through the top and bottom ferrite materials are shown in Fig. 8 (a) and Fig. 9 (a) respectively. The evolution of the magnetic field  $H_i$  in the middle of the upper and lower ferrite substrates along the X and Y axis is reported in Fig. 8 (b) and Fig. 9 (b), respectively.

The internal magnetic field varies between 550 Oe and 651 Oe for the upper ferrite and remains nearly constant

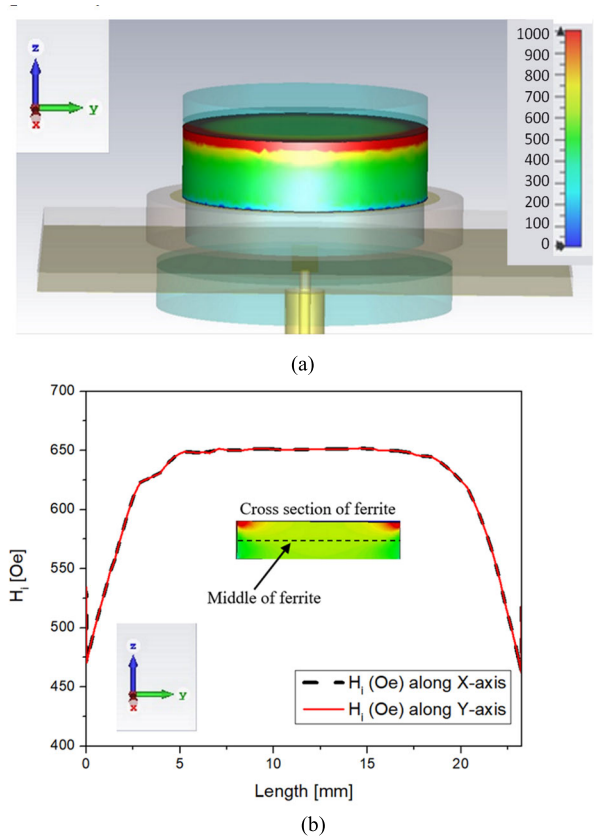


FIGURE 8. Magnetic field distribution inside the upper ferrite substrate: (a) 3D view, and (b) variation of the internal magnetic field in the middle of the ferrite substrate along X and Y axis.

at around 650 Oe in a large part of the ferrite (Fig. 8 (b)), indicating that the target value (650 Oe) for the upper ferrite is accurately achieved. Similarly, Fig. 9 (b) shows that the magnetic field inside the lower ferrite varies between 620 Oe and 676 Oe, with a stable value of around 620 Oe in a large part of the ferrite, which is close to the targeted 620 Oe.

Now that the magnetic field has been simulated, it can be imported into the electromagnetic simulation of the antenna in order to determine the antenna's performance under real magnetic field conditions. A detailed description of the antenna's performance is presented in the next section.

### C. MAGNETOSTATIC/ELECTROMAGNETIC CO-SIMULATION OF THE ANTENNA

This section presents the antenna's performance under an inhomogeneous magnetic field, derived from the magnetostatic simulation with permanent magnets.

Similar to the ideal case, a matching criterion of  $-6$  dB is used. Fig. 10 (a) and (b) show that the antenna remains well matched around 1.227 GHz and 1.575 GHz. The boresight axial ratio is well below 3 dB across the entire impedance bandwidths with minimum values of 0.33 dB at 1.227 GHz and 1.54 dB at 1.575 GHz. Impedance bandwidths of 9.45 MHz (0.77%) and 51.2 MHz (3.25%) were respectively obtained at the 1<sup>st</sup> and 2<sup>nd</sup> RHCP modes.

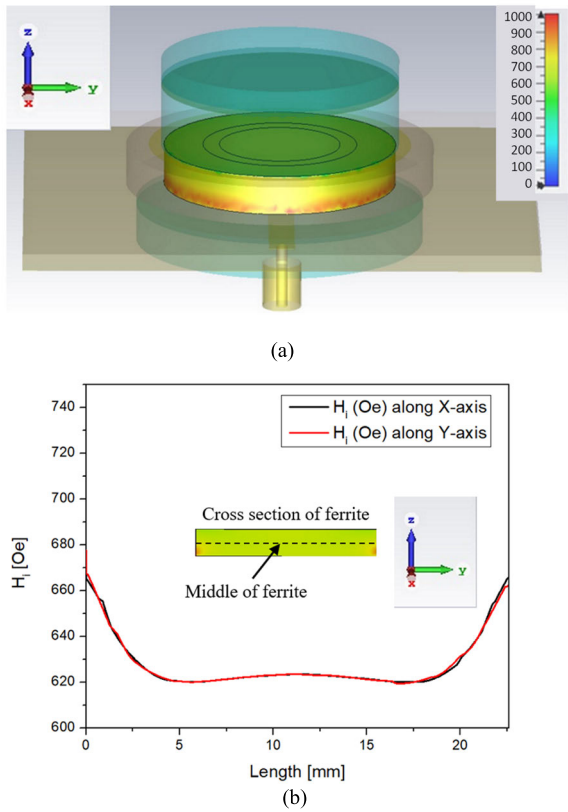


FIGURE 9. Magnetic field distribution inside the lower ferrite substrate: (a) 3D view, and (b) variation of the internal magnetic field in the middle of the ferrite substrate along X and Y axis.

The compact size of the antenna at the 1<sup>st</sup> RHCP mode, combined with the high dielectric constant of the ferrite (Y39), results in a lower impedance bandwidth. Enhancing the impedance bandwidth using a wideband matching network is feasible; however, implementing such a network on a Rogers RT5880 substrate would make the structure more complex. It was not pursued in this study, as the primary focus was on achieving identical circular polarization modes.

The results obtained under non-uniform magnetic fields are close to the ideal-case results and validate the magnets selected for use in the rest of this work.

Fig. 11 shows the normalized radiation performance of the antenna in a real magnetic field environment. Fig. 6 (uniform magnetic field) and Fig. 11 (non-uniform magnetic field) show that the radiation performance of the antenna is identical in the “ideal” and “real” magnetic field conditions, since in both cases the RHCP mode is identified as the co-polarization of the antenna at the operating frequencies.

The realized gains and radiation efficiencies of the antenna are  $-1.82$  dBi and 33.6%, respectively, for the 1<sup>st</sup> RHCP mode (1.227 GHz) and 2.77 dBi and 62%, respectively, for the 2<sup>nd</sup> RHCP mode (1.575 GHz).

In the 1<sup>st</sup> RHCP mode, the electric field is distributed across both ferrite resonators, rather than being confined to a single resonator, forming a volume mode. This distribution increases the total magnetic losses, as both ferrite

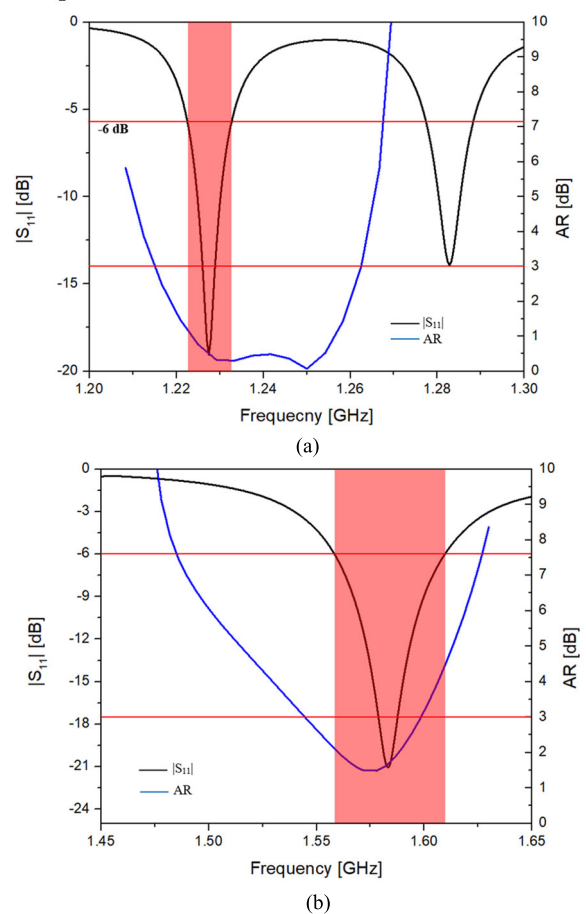


FIGURE 10.  $|S_{11}|$  and AR of the antenna for non-uniform magnetic field inside the ferrite material: (a) 1<sup>st</sup> RHCP mode and (b) 2<sup>nd</sup> RHCP mode.

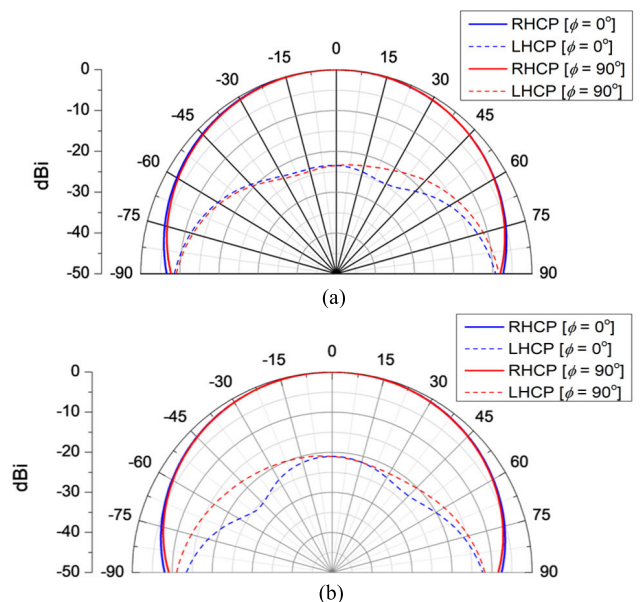


FIGURE 11. Normalized radiation patterns for  $\phi = 0^\circ$  (xOz-plane) and  $\phi = 90^\circ$  (yOz-plane): (a) at 1.227 GHz, and (b) at 1.575 GHz.

resonators contribute to the losses, resulting in reduced efficiency. Consequently, the volumetric nature of this mode

is responsible for the observed decrease in both efficiency and realized gain. The 2<sup>nd</sup> RHCP mode operates close to the gyromagnetic resonance (1.820 GHz), which slightly increases magnetic losses, leading to a minor reduction in both efficiency and realized gain.

The next step is to experimentally validate the simulated results through prototype measurement.

**IV. PROTOTYPE FABRICATION**

The metallic etching of the patches was performed using a photolithography process (Fig. 12). The first step consisted of depositing a Ti/Au (20/200 nm) layer by e-beam evaporation on the ferrite substrate (Fig. 12). Then, a gold electroplating step was performed to obtain a metallic thickness of at least 8 μm, which is greater than three times the skin depth of gold (2.6 μm) at the L-band, thereby reducing metal-related losses. The patches were etched using a photolithography step with a positive (photosensitive) resin followed by wet etching.

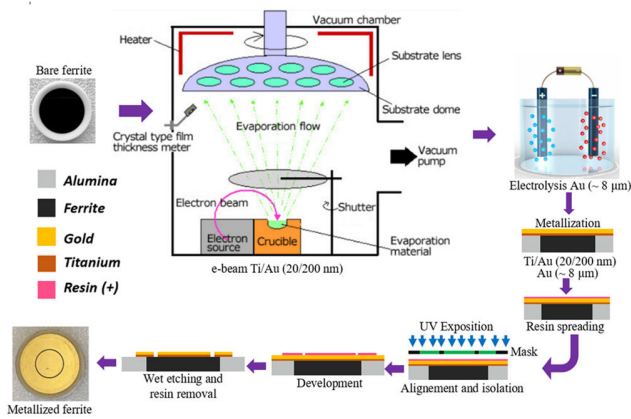


**FIGURE 12.** Photolithography process of metallization on ferrite substrate.

The Rogers substrate incorporates both the ground plane and the feeding line. The final antenna prototype is depicted in Fig. 13. Proper alignment of all these layers was achieved by placing them inside a dedicated Rohacell structure, as shown in Fig. 14.

**V. MEASUREMENT**

The radiation performance of the antenna was measured inside an anechoic chamber using an optical RF converter to excite the antenna (Fig. 14). Using an RF optical converter in the antenna measurement process eliminates the surface currents that exist on a conventional cable [32].

Fig. 15 shows the measured S-parameters and boresight axial ratio, indicating frequency shifts of 3% and 2.2% for the 1<sup>st</sup> (1.265GHz) and 2<sup>nd</sup> (1.545GHz) RHCP modes of the antenna compared with the simulation results. This small discrepancy may result from a ±5% variation in ε<sub>r</sub> of the ferrite, a lower magnetic flux density of the magnets than assumed in simulation, and/or air gaps introduced by the insertion of the ferrite into the dielectric ring.

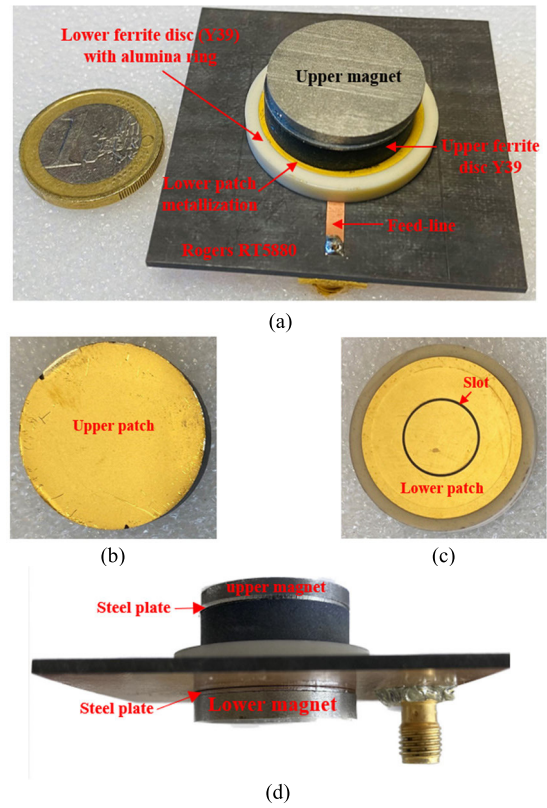


**FIGURE 13.** (a) Proposed antenna prototype, (b) lower patch on the lower ferrite disc, (c) upper patch on the upper ferrite disc, and (d) side view of the complete prototype.

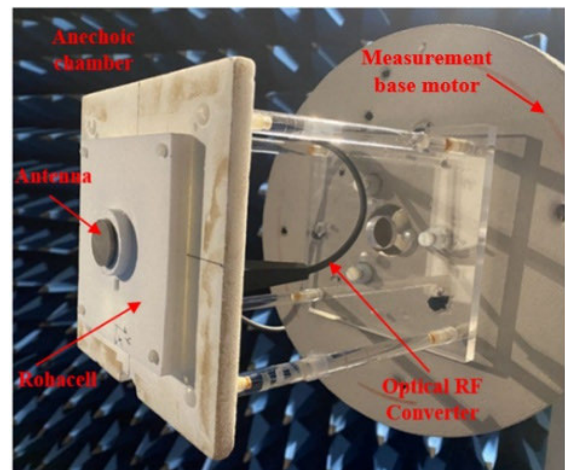


**FIGURE 14.** Antenna with rohacell structure in measurement set-up.

Good impedance matching is obtained as well as a good boresight axial ratio, since it remains below 3 dB within the frequency bands where the antenna has a |S<sub>11</sub>| lower than -6 dB.

Fig. 16 shows the measured normalized right and left polarization at the frequencies 1.265 GHz and 1.545 GHz for two cutting planes, φ = 0° and φ = 90°. The authenticity of the RHCP mode as co-polarization and the LHCP

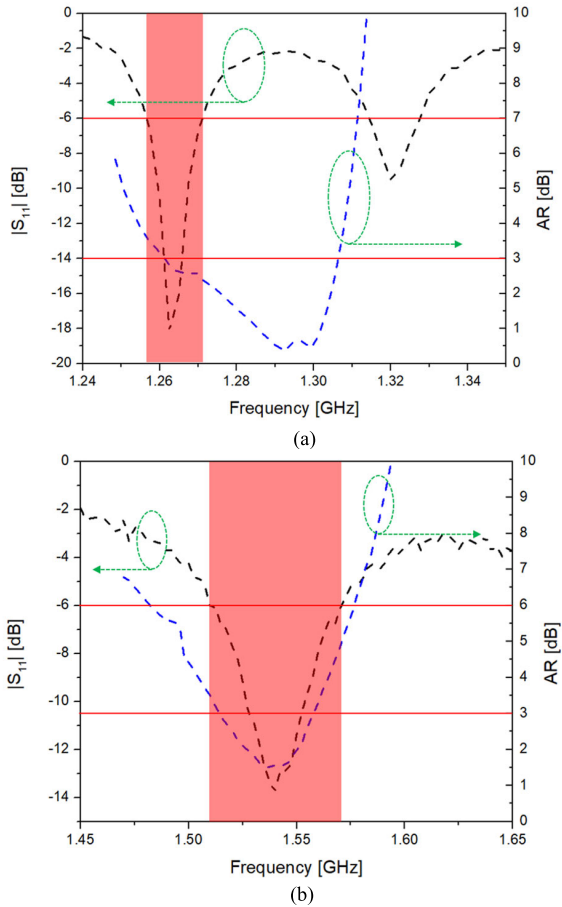


FIGURE 15. Measured  $|S_{11}|$  and AR of the antenna: (a) 1<sup>st</sup> RHCP mode, and (b) 2<sup>nd</sup> RHCP mode.

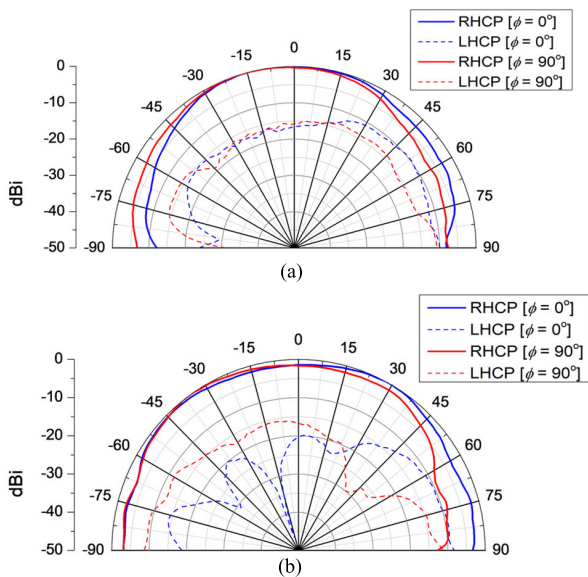


FIGURE 16. Measured normalized radiation patterns for  $\phi = 0^\circ$  (xOz-plane) and  $\phi = 90^\circ$  (yOz-plane): (a) at 1.265 GHz, and (b) at 1.545 GHz.

mode as cross-polarization in the measurements is therefore confirmed. The level of cross-polarization is approximately

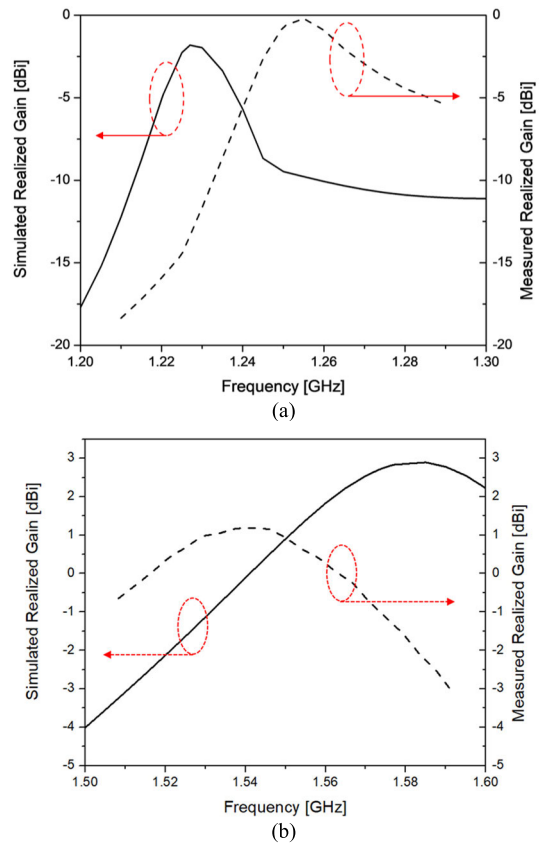


FIGURE 17. Simulated and measured gain of the antenna: (a) at 1<sup>st</sup> RHCP mode, (b) at 2<sup>nd</sup> RHCP mode.

TABLE 1. Comparison of simulated and measured antenna characteristics.

Antenna Characteristics	Co-Simulation	Measurement
$f_o$ at 1 <sup>st</sup> RHCP mode	1.227 GHz	1.265 GHz
$f_o$ at 2 <sup>nd</sup> RHCP mode	1.575 GHz	1.545 GHz
Impedance Bandwidth at 1 <sup>st</sup> RHCP mode	9.45 MHz (0.77%)	12.5 MHz (0.99%)
Impedance Bandwidth at 2 <sup>nd</sup> RHCP mode	51.2 MHz (3.25%)	60 MHz (3.88%)
Axial Ratio at 1 <sup>st</sup> RHCP mode	0.33 dB	2.57 dB
Axial Ratio at 2 <sup>nd</sup> RHCP mode	1.54 dB	1.61 dB
Maximum Realized gain at 1 <sup>st</sup> RHCP mode	-1.82 dBi at 1.227 GHz	-0.2 dBi at 1.265 GHz
Maximum Realized gain at 2 <sup>nd</sup> RHCP mode	2.77 dBi at 1.575 GHz	1.16 dBi at 1.545 GHz
Radiation efficiency at 1 <sup>st</sup> RHCP mode	33.6%	27%
Radiation efficiency at 2 <sup>nd</sup> RHCP mode	62%	57%

15 dB lower than that of the RHCP mode in both planes, at 1.265 GHz and 1.545 GHz.

**TABLE 2. Comparison of the proposed antenna design and previously reported non-ferrite and ferrite antenna structures.**

Reference	$f_o$ (GHz)	Operating Mode	Antenna Dimensions at 1 <sup>st</sup> $f_o$ (excluding ground plane size)	Antenna Dimensions at 1 <sup>st</sup> $f_o$ (including ground plane size)	AR (dB)	Gain (dBi/dBic)
Non-Ferrite Single-Band Microstrip Patch Antennas						
[1]	3	RHCP	$\frac{\lambda_0}{3.8} \times \frac{\lambda_0}{3.8}$	$\frac{\lambda_0}{2.3} \times \frac{\lambda_0}{2.3}$	<3	5.1 dBiC
[2]	1.807	LHCP	$\frac{\lambda_0}{5.53} \times \frac{\lambda_0}{5.53} \times \frac{\lambda_0}{103.76}$	NA	1.2	-
[3]	1.575	RHCP	$\frac{\lambda_0}{3.26} \times \frac{\lambda_0}{3.26} \times \frac{\lambda_0}{125}$	NA	1.8	6 dBic
[5]	1.575	LHCP/RHCP	$\frac{\lambda_0}{5.4} \times \frac{\lambda_0}{3.9} \times \frac{\lambda_0}{59.5}$	$\frac{\lambda_0}{3.5} \times \frac{\lambda_0}{2.9} \times \frac{\lambda_0}{59.5}$	<1	5 dBi
Non-Ferrite Dual-Band Microstrip Patch Antennas						
[1]	2.86 3.11	LHCP RHCP	$\frac{\lambda_0}{4.03} \times \frac{\lambda_0}{4.03}$	$\frac{\lambda_0}{2.41} \times \frac{\lambda_0}{2.41}$	0.84 1.26	4.15 dBic 4.77 dBic
[6]	2.5 3.5	RHCP LHCP	NA	$\frac{\lambda_0}{1.62} \times \frac{\lambda_0}{1.71} \times \frac{\lambda_0}{40}$	<3	6.52 dBic 7.04 dBic
[7]	2.1 2.2	CP	$\frac{\lambda_0}{4.33} \times \frac{\lambda_0}{4.67} \times \frac{\lambda_0}{44.64}$	NA	<2.5	<4 dBi
[8]	2.134 2.223	LHCP RHCP	$\frac{\lambda_0}{2.42} \times \frac{\lambda_0}{3.26} \times \frac{\lambda_0}{46.86}$	$\frac{\lambda_0}{1.28} \times \frac{\lambda_0}{1.28} \times \frac{\lambda_0}{46.86}$	<3	7.5 dBic
[9]	1.227 1.575	RHCP RHCP	$\frac{\lambda_0}{1.76} \times \frac{\lambda_0}{1.76} \times \frac{\lambda_0}{43.7}$	NA	$\cong 1$	6.78 dBi 6.46 dBi
[13]	1.9 2.3	RHCP LHCP	NA	$\frac{\lambda_0}{1.75} \times \frac{\lambda_0}{1.75} \times \frac{\lambda_0}{194.2}$	<3	4.3 dBic 5.3 dBic
[14]	1.227 1.575	RHCP RHCP	$\frac{\lambda_0}{10} \times \frac{\lambda_0}{10} \times \frac{\lambda_0}{25}$	$\frac{\lambda_0}{4.9} \times \frac{\lambda_0}{4.9} \times \frac{\lambda_0}{25}$	<3	1.57 dBic 3.02 dBic
Ferrite Microstrip Patch Antennas						
[17]	4.6 5.31	RHCP LHCP	$\frac{\lambda_0}{4.4} \times \frac{\lambda_0}{4.4} \times \frac{\lambda_0}{21.4}$	$\frac{\lambda_0}{2.3} \times \frac{\lambda_0}{1.6} \times \frac{\lambda_0}{21.4}$	4.25 2.63	-5 dBi
[21]	2.025 $\cong 2.2$	RHCP LHCP	$\frac{\lambda_0}{8.5} \times \frac{\lambda_0}{8.5} \times \frac{\lambda_0}{37}$	$\frac{\lambda_0}{2.9} \times \frac{\lambda_0}{2.9} \times \frac{\lambda_0}{37}$	$\cong 3$	5.25 dBi
[22]	3.3 3.9 7.54	RHCP LHCP RHCP	$\frac{\lambda_0}{9.1} \times \frac{\lambda_0}{8.6} \times \frac{\lambda_0}{22.7}$	$\frac{\lambda_0}{4.5} \times \frac{\lambda_0}{4.5} \times \frac{\lambda_0}{22.7}$	0.4 1 2.8	1.8 dBic 2.6 dBic 3.7 dBic
This work	1.265 1.545	RHCP RHCP	$\frac{\lambda_0}{9.1} \times \frac{\lambda_0}{9.1} \times \frac{\lambda_0}{22.4}$	$\frac{\lambda_0}{4.7} \times \frac{\lambda_0}{4.7} \times \frac{\lambda_0}{22.4}$	2.57 1.61	-0.2 dBi 1.16 dBi

The maximum realized gain of the antenna was measured and compared with the simulation results, as presented in Fig. 17. Due to the frequency shift of the two RHCP modes observed in measurement, a similar offset is also evident in the measured realized gain. A maximum realized gain of -0.2 dBi and 1.16 dBi was obtained in measurement at 1.265 GHz and 1.545 GHz, respectively.

Table 1 summarizes the antenna’s performance in both measurement and co-simulation. This table shows that the antenna exhibits consistent behavior in co-simulation and measurement.

The measured gain for the 1<sup>st</sup> RHCP mode appears higher than the simulated result. Replicating the measurement conditions in simulations is challenging, particularly due to the antenna’s compact size and small ground plane, which

complicate direct gain comparisons. The measurement base motor (Fig. 14) located behind the ground plane, influences radiation. Therefore, a retro-simulation including a metal plate behind the ground plane was performed to mimic this effect. A simplified representation of the motor's presence increases the simulated gain (the realized gain from retro-co-simulation is around 0 dBi), although it still remains slightly higher than the measured value.

The significantly lower measured gain for the 2<sup>nd</sup> RHCP mode was analyzed to clarify the cause of this discrepancy. Magnetic losses in ferrites are modeled far from the gyroresonance using the parameter  $\Delta H_{eff}$  (4 Oe for the material used in simulation) and near the gyroresonance using the parameter  $\Delta H$  (40 Oe for the material used in simulation). A DC bias of 650 Oe is applied to the upper ferrite to achieve RHCP at 1.575 GHz, with gyroresonance occurring at 1.82 GHz. Setting  $\Delta H_{eff}$  to 4 Oe in the model underestimates losses, since the antenna operates in an intermediate zone, not exactly at gyroresonance, but not far from it either. An intermediate loss value (between  $\Delta H$  and  $\Delta H_{eff}$ ) better represents this case; using  $\Delta H_{eff} = 10$  Oe yields a simulated gain of 1.24 dBi at 1.55 GHz, closely matching the measured gain of 1.16 dBi at 1.545 GHz. A comparison of the characteristics and dimensions of the proposed antenna with existing designs in the literature is presented in Table 2.

The ground plane size critically affects patch antenna performance, influencing parameters such as radiation pattern, gain, bandwidth, and overall dimensions. In this work, we evaluated the impact of ground plane dimensions by comparing a 50 mm  $\times$  50 mm configuration with a smaller 30 mm  $\times$  30 mm one, which covers only the resonators. The results show that the ground plane size does not affect the  $|S_{11}|$  parameter, as the resonances are primarily governed by the ferrite resonators dimensioned through a modal study. However, the gain decreases by approximately 1-1.5 dB on both operating bands when the smaller ground plane is used. Consequently, the 50 mm  $\times$  50 mm ground plane was selected as a trade-off, ensuring reduced measurement perturbations while maintaining compact antenna dimensions.

This work follows prior studies [1], [2], [3], [5], [14], [21], [22] that report compact antennas excluding ground plane size. Thus, the antenna dimensions presented here exclude the ground plane. Table 2 compares non-ferrite and ferrite designs (available in the literature) with and without ground planes, showing that the proposed antenna remains compact in both cases despite its greater height.

The table clearly indicates that non-ferrite antennas exhibit higher gain than the proposed antenna. This difference is primarily due to the following factors:

- i. The compact size of the proposed antenna.
- ii. The magnetic losses it incurs, and the absence of such magnetic losses in non-ferrite antennas.

A detailed loss analysis, presented in Table 3, shows radiation efficiency is mainly limited by magnetic losses.

Simulations considering only magnetic losses yield efficiencies of 37% at 1.227 GHz and 64% at 1.575 GHz, whereas simulations including all losses result in 33.6% and 62%, respectively, confirming the dominant influence of magnetic losses.

**TABLE 3. Radiation efficiency of the proposed antenna with and without losses.**

Operating Frequency [GHz]	Radiation efficiency without loss (%)	Radiation efficiency with only magnetic losses (%)	Radiation Efficiency with all losses (%) (dielectric + metallic + magnetic losses)
1.227	100	37	33.6
1.575	100	64	62

Another important observation is that the ferrite-free antenna reported in [14], although similar in size to the proposed design, exhibits a higher gain but excludes feed network losses in both simulation and measurement. In contrast, the proposed antenna accounts for all losses, providing more accurate and realistic gain values. Furthermore, when feed network losses are considered in the design from [14], the authors of this work achieve nearly identical results using a different technology.

Table 2 shows that prior ferrite-based antennas [17], [21], [22] exhibit contra-rotating modes at their operating frequencies, whereas the proposed design produces only RHCP modes across all operating frequencies, introducing a novel feature. It also achieves equal or superior miniaturization compared to existing designs and exhibits lower axial ratios than those reported in [17] and [21].

The key factors contributing to the lower gain of the proposed ferrite antenna compared to other ferrite antennas [17], [21], [22] are as follows:

- i The proposed antenna is more compact than those described in [17] and [21].
- ii At the 1<sup>st</sup> RHCP mode (1.227 GHz in simulation), the electric field distribution across both resonators resembles a volume mode, resulting in increased magnetic losses. Since both ferrite resonators contribute to these losses, this leads to reduced efficiency and realized gain.
- iii The proximity between the 2<sup>nd</sup> resonance and the gyroresonance in the proposed antenna is similar to that observed in [22], but closer than in [21], resulting in magnetic losses comparable to [22] and potentially higher than [21].
- iv Partial ferrite use, as implemented in [17], effectively reduces magnetic losses. In contrast, the proposed antenna employs nearly two stacked all-ferrite substrates (100% and 75% Y39 for the upper and lower layers, respectively), which leads to higher magnetic losses and, consequently, lower gain than the design in [17].

## VI. CONCLUSION

Typically, magnetized ferrite antennas exhibit multiband behavior with counter-rotating modes that produce right- or left-hand circularly polarized radiations depending on the mode that is excited. The authors of this paper have taken the opportunity to modify this basic characteristic of ferrite-based antennas.

The main objective was to generate two RHCP modes at two closely spaced operating frequencies using a polarized ferrite material. This goal was achieved by proposing a unique topology consisting of two stacked ferrite disks. By creating circular patches of different diameters on the lower and upper ferrite disks, and by providing different internal DC magnetic fields inside the lower and upper ferrite substrates, the authors succeeded in obtaining for the first time the RHCP mode at two close frequencies for L-band applications. The high dielectric constant of the ferrite material and the high effective permeability (greater than 1 in the strong-field region) enabled significant miniaturization of the antenna structure.

The RHCP modes were matched to the successive operating frequencies of the antenna (1.227 GHz and 1.575 GHz) in the presence of both homogeneous and non-uniform DC magnetic fields in simulation. The axial ratio of less than 2 dB confirmed the excitation of circular polarization in the antenna. Validation of the simulation results was achieved by fabricating and measuring the prototype antenna. The measurements confirmed dual-band behavior with only RHCP modes and a good axial ratio. Compared with existing ferrite-based antennas, the proposed design represents a significant advance, as it produces two identical modes (only RHCP). In addition, this topology maximizes the miniaturization of the antenna structure and therefore has great potential for use as a compact circularly polarized (RHCP-only) antenna for L-band applications.

Although the antenna demonstrates excellent polarization purity and compactness, its impedance bandwidth remains relatively narrow. Future work could focus on integrating a wideband matching network to improve impedance matching and on exploring operation in regions where the effective permeability becomes negative, in order to broaden the axial-ratio bandwidth.

## ACKNOWLEDGMENT

The current work was carried out in the framework of the Joint Laboratory INOgyRO (<https://inogyro.xlim.fr/>) associating the Research Institution XLIM with the SME INOVEOS.

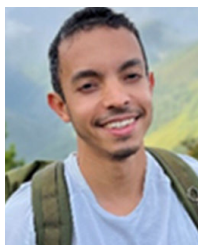
## REFERENCES

- [1] H.-X. Xu, G.-M. Wang, J.-G. Liang, M. Q. Qi, and X. Gao, "Compact circularly polarized antennas combining meta-surfaces and strong space-filling meta-resonators," *IEEE Trans. Antennas Propag.*, vol. 61, no. 7, pp. 3442–3450, Jul. 2013.
- [2] H. Oraizi and S. Hedayati, "Miniaturization of microstrip antennas by the novel application of the giuseppe peano fractal geometries," *IEEE Trans. Antennas Propag.*, vol. 60, no. 8, pp. 3559–3567, Aug. 2012.
- [3] K. S. Rao, D. R. Jahagirdar, and D. Ramakrishna, "Compact broadband asymmetric slit circularly polarized microstrip patch antenna for GPS and GLONASS applications," in *Proc. IEEE Int. Conf. Antenna Innov. Modern Technol. Ground, Aircr. Satell. Appl.*, Bengaluru, India, Nov. 2017, pp. 1–3.
- [4] Z. Ning Chen, X. Qing, and H. Leong Chung, "A universal UHF RFID reader antenna," *IEEE Trans. Microw. Theory Techn.*, vol. 57, no. 5, pp. 1275–1282, May 2009.
- [5] M. S. Nishamol, V. P. Sarin, D. Tony, C. K. Aanandan, P. Mohanan, and K. Vasudevan, "Design of a circularly polarized rectangular microstrip antenna for GPS applications," *Microw. Opt. Technol. Lett.*, vol. 53, no. 2, pp. 468–470, Feb. 2011.
- [6] K. Li, L. Li, Y.-M. Cai, C. Zhu, and C.-H. Liang, "A novel design of low-profile dual-band circularly polarized antenna with metasurface," *IEEE Antennas Wireless Propag. Lett.*, vol. 14, pp. 1650–1653, 2015.
- [7] S. Kumar, B. K. Kanaujia, M. K. Khandelwal, and A. K. Gautam, "Stacked dual-band circularly polarized microstrip antenna with small frequency ratio," *Microw. Opt. Technol. Lett.*, vol. 56, no. 8, pp. 1933–1937, Aug. 2014.
- [8] N.-W. Liu, L. Zhu, Z.-X. Liu, Z.-Y. Zhang, and G. Fu, "Frequency-ratio reduction of a low-profile dual-band dual-circularly polarized patch antenna under triple resonance," *IEEE Antennas Wireless Propag. Lett.*, vol. 19, pp. 1689–1693, 2020.
- [9] A. A. Heidari, M. Heyrani, and M. Nakhkash, "A dual-band circularly polarized stub loaded microstrip patch antenna for gps applications," *Prog. Electromagn. Res.*, vol. 92, pp. 195–208, 2009.
- [10] K.-P. Yang and K.-L. Wong, "Dual-band circularly-polarized square microstrip antenna," *IEEE Trans. Antennas Propag.*, vol. 49, no. 3, pp. 377–382, Mar. 2001.
- [11] F. Fezai, A. A. Nour, J. Sence, T. Monediere, F. Torres, R. Chantalat, S. Bila, and B. Jarry, "Low-profile dual-band circularly polarized microstrip antenna for GNSS applications," in *Proc. 9th Eur. Conf. Antennas Propag. (EuCAP)*, Lisbon, Portugal, Apr. 2015, pp. 1–4.
- [12] M.-J. Hou and J.-S. Row, "Compact circularly polarized microstrip antenna for GPS applications," *Microw. Opt. Technol. Lett.*, vol. 56, no. 6, pp. 1293–1296, Jun. 2014.
- [13] W. Wang, C. Chen, and W. Wu, "Low-profile dual-band dual circularly polarized patch antenna with small frequency ratio," *Int. J. RF Microw. Comput.-Aided Eng.*, vol. 31, no. 10, Oct. 2021, Art. no. e22806.
- [14] M.-S. Wang, X.-Q. Zhu, Y.-X. Guo, and W. Wu, "Miniaturized dual-band circularly polarized quadruple inverted-F antenna for GPS applications," *IEEE Antennas Wireless Propag. Lett.*, vol. 17, pp. 1109–1113, 2018.
- [15] D. M. Pozar and S. M. Duffy, "A dual-band circularly polarized aperture-coupled stacked microstrip antenna for global positioning satellite," *IEEE Trans. Antennas Propag.*, vol. 45, no. 11, pp. 1618–1625, Nov. 1997.
- [16] F. Bilotti and C. Vegni, "Design of high-performing microstrip receiving GPS antennas with multiple feeds," *IEEE Antennas Wireless Propag. Lett.*, vol. 9, pp. 248–251, 2010.
- [17] E. Andreou, T. Zervos, A. A. Alexandridis, and G. Fikioris, "Magnetodielectric materials in antenna design: Exploring the potentials for reconfigurability," *IEEE Antennas Propag. Mag.*, vol. 61, no. 1, pp. 29–40, Feb. 2019.
- [18] E. Andreou, T. Zervos, F. Lazarakis, A. A. Alexandridis, K. Dangakis, E. Varouti, G. Fikioris, and J. C. Vardaxoglou, "Reconfigurable proximity coupled patch antenna using magnetic bias," in *Proc. Loughborough Antennas Propag. Conf. (LAPC)*, Nov. 2014, pp. 376–380.
- [19] T. Zervos, A. A. Alexandridis, F. Lazarakis, and K. Dangakis, "Patch antenna with polarization agility using ferrimagnetic materials," in *Proc. Loughborough Antennas Propag. Conf.*, Nov. 2009, pp. 541–544.
- [20] M. Sigalov, R. Shavit, and E. O. Kamenetskii, "Dual band circular polarized patch antenna using small ferrite disks," *Proc. 25th Conv. Electr. Electron. Engineers*, vol. 74, pp. 523–527, Mar. 2008.
- [21] E. Arnaud, L. Huitema, R. Chantalat, A. Bellion, and T. Monediere, "Miniaturization of a circular polarized antenna using ferrite materials," in *Proc. 12th Eur. Conf. Antennas Propag. (EuCAP)*, Apr. 2018, pp. 1–5.
- [22] S. Jemmel, T. Monediere, E. Arnaud, and L. Huitema, "Design of a miniature circularly polarized antenna operating in three frequency bands using a polarized ferrite material," *IEEE Trans. Antennas Propag.*, vol. 69, no. 8, pp. 4304–4312, Aug. 2021.
- [23] S. Jemmel, T. Monediere, E. Arnaud, and L. Huitema, "Ultra-miniature and circularly polarized ferrite patch antenna," *IEEE Trans. Antennas Propag.*, vol. 71, no. 8, pp. 6435–6443, Aug. 2023.

- [24] D. M. Pozar, "Radiation and scattering characteristics of microstrip antennas on normally biased ferrite substrates," *IEEE Trans. Antennas Propag.*, vol. 40, no. 9, pp. 1084–1092, Sep. 1992.
- [25] *CST Studio Suite*. Dassault Systèmes. Accessed: Oct. 17, 2025. [Online]. Available: <https://www.3ds.com/products/simulia/cst-studio-suite>
- [26] G. T. Rado, "Theory of the microwave permeability tensor and Faraday effect in nonsaturated ferromagnetic materials," *Phys. Rev.*, vol. 89, no. 2, p. 529, Jan. 1953.
- [27] J. J. Green and F. Sandy, "Microwave characterization of partially magnetized ferrites," *IEEE Trans. Microw. Theory Techn.*, vol. MTT-22, no. 6, pp. 641–645, Jun. 1974.
- [28] M. Igarashi and Y. Naito, "Tensor permeability of partially magnetized ferrites," *IEEE Trans. Magn.*, vol. M-13, no. 5, pp. 1664–1668, Sep. 1977.
- [29] M. Igarashi and Y. Naito, "Parallel component  $\mu_{\text{sub } z}$  of partially magnetized microwave ferrites," *IEEE Trans. Microw. Theory Techn.*, vol. MTT-29, no. 6, pp. 568–571, Jun. 1981.
- [30] *Cermag Magnets*. Accessed: Oct. 17, 2025. [Online]. Available: <https://cermagmagnets.co.uk/>
- [31] H. Turki, L. Huitema, T. Monediere, B. Lenoir, and C. Breuil, "New concept validation of low-loss dual-band stripline circulator," *IEEE Trans. Microw. Theory Techn.*, vol. 67, no. 3, pp. 845–850, Mar. 2019.
- [32] L. Huitema, C. Delavaud, and R. D'Errico, "Impedance and radiation measurement methodology for ultra miniature antennas," *IEEE Trans. Antennas Propag.*, vol. 62, no. 7, pp. 3463–3473, Jul. 2014.



**WRIDDHI BHOWMIK** was born in India, in 1985. He received the M.E. and Ph.D. degrees in electronics and communication engineering from Birla Institute of Technology, Mesra, Ranchi, India, in 2010 and 2017, respectively. From 2020 to 2021, he was a Postdoctoral Scientist with the XLIM Research Institute, University of Limoges, France. He is currently an Assistant Professor with the School of Electronics Engineering, KIIT Deemed to be University, Bhubaneswar, India. His research interests include the design of beamforming networks (Butler matrix array), SIW horn antenna arrays, magnetized ferrite antennas with circular polarization, MIMO antennas, and terahertz metamaterial absorbers for biosensing applications.



**JEHISON LEON VALDES** received the M.S. and Ph.D. degrees in telecommunications, high frequencies, and optics from the University of Limoges, Limoges, France, in 2017 and 2020, respectively. He is currently a Postdoctoral Research Fellow with the Antennas and Signals Team, RF Systems Axis, XLIM Research Institute. His research interests include circularly polarized, reconfigurable, miniature, and multiband antennas using ferrite materials and phase change materials.



**THIERRY MONEDIERE** was born in Tulle, France, in 1964. He received the Ph.D. degree from the IRCOM Laboratory, University of Limoges, Limoges, France, in 1990. He is currently a Professor with the Antennas and Signals Team, XLIM Research Laboratory, University of Limoges. He develops his research activities in this laboratory and works on multifunction antennas, miniature antennas, antenna arrays, and active antennas. He also studies gyromagnetic devices as ferrite circulators or isolators.



**LAURE HUITEMA** (Member, IEEE) received the M.S. and Ph.D. degrees in telecommunications, high frequencies, and optics from the University of Limoges, France, in 2008 and 2011, respectively. From 2011 to 2012, she was a Postdoctoral Research Fellow with the Atomic Energy Commission (CEA), Laboratory of Electronics and Information Technology (LETI), Grenoble, France. She is currently an Associate Professor with the Antennas and Signals Team, RF Systems Axis, XLIM Research Institute, University of Limoges. Since 2024, she has been with the Institut Universitaire de France (IUF). More recently, she has been working on the integration of new components based on innovative materials for their integration into antennas, and was the project leader of a European H2020 project called MASTERS ([http://www.unilim.fr/H2020\\_MASTERS/](http://www.unilim.fr/H2020_MASTERS/)). Since 2019, she has been the Director of the Joint Laboratory INOgyro, which groups together the Xlim laboratory and the company Inoveos (<https://inogyro.xlim.fr/>). Her research interests include reconfigurable antennas, dielectric resonator antennas, miniature antennas, multiband antennas, and circulators. She received the Best Student Paper Award at the IEEE International Workshop on Antenna Technology (IWAT), in 2010, and the Best Student Paper Award at the JCMM 2010 Conference. In 2020, she was also awarded the Bronze Medal of the French National Center for Scientific Research (CNRS).

• • •